Epidemic spreading on modular networks: The fear to declare a pandemic

Lucas D. Valdez [1,*] Lidia A. Braunstein [2,1] and Shlomo Havlin[3,1,4]

[1]*Department of Physics, Boston University, Boston, Massachusetts 02215, USA*
[2]*Instituto de Investigaciones Físicas de Mar del Plata (IFIMAR)-Departamento de Física, FCEyN, Universidad Nacional de Mar del Plata-CONICET, Mar del Plata 7600, Argentina*
[3]*Department of Physics, Bar Ilan University, Ramat Gan 5290002, Israel*
[4]*Tokyo Institute of Technology, Yokohama 152-8550, Japan*

In the past few decades, the frequency of pandemics has been increased due to the growth of urbanization and mobility among countries. Since a disease spreading in one country could become a pandemic with a potential worldwide humanitarian and economic impact, it is important to develop models to estimate the probability of a worldwide pandemic. In this paper, we propose a model of disease spreading in a structural modular complex network (having communities) and study how the number of bridge nodes n that connect communities affects disease spread. We find that our model can be described at a global scale as an infectious transmission process between communities with global infectious and recovery time distributions that depend on the internal structure of each community and n. We find that near the critical point as n increases, the disease reaches most of the communities, but each community has only a small fraction of recovered nodes. In addition, we obtain that in the limit $n \to \infty$, the probability of a pandemic increases abruptly at the critical point. This scenario could make the decision on whether to launch a pandemic alert or not more difficult. Finally, we show that link percolation theory can be used at a global scale to estimate the probability of a pandemic since the global transmissibility between communities has a weak dependence on the global recovery time.

I. INTRODUCTION

Community or modular structure is a ubiquitous property in real complex networks that can be found in systems such as brain networks, social networks, and technological networks [1–3]. A community is a subgraph with more internal than external connections, and as the number of internal links increases compared to the external ones, the network has a higher level of community structure or modularity [1,4]. Several theoretical studies have focused on studying models of networks with subgraphs whose nodes are densely connected in order to understand the effect of the community structure on processes that develop on top of complex networks [5–8]. Disease spreading is one of the most studied dynamic processes since many diseases that emerge could become an epidemic, i.e., could affect a large number of people, or even could spread across the world and become a pandemic. Nowadays, due to the enhanced human migration from rural to urban regions [9,10], many people live in agglomerated cities throughout the planet where the number of internal contacts is much higher than the number of contacts among people from different cities. When a disease spreads between different cities or regions, it is essential for national and international health authorities to activate mitigation or immunization strategies, when a disease is a small outbreak, an epidemic, or even a pandemic. Therefore, developing models

is crucial to predict the epidemic and pandemic potential of a disease spreading and for developing mitigation strategies.

The susceptible-infected-recovered (SIR) model is widely used to study diseases that confer permanent immunity [11]. In this model, the nodes can be in one of the following states: (1) susceptible, i.e., a node that is healthy but not immunized to the disease; (2) infected and thus can transmit the disease to its susceptible neighbors; and (3) recovered, which is a node that cannot transmit the disease because it acquired permanent immunity. For a discrete-time evolution, the dynamic rules of the SIR model are as follows: An infected individual tries to infect a susceptible neighbor with probability β per unit time step and recovers after a fixed recovery time, t_r, that could be the same for all nodes or follow a probability distribution $P(t_r)$ [12,13]. A relevant parameter of this model is the transmissibility T, which is the effective transmission or infection probability and depends on β and t_r [14]. At the initial state of the dynamic process, all the nodes are susceptible except for one infected node called the index case, from where the disease might spread throughout the network. During the early stages of the dynamic process, there are only a few infected nodes, and hence the process is in a stochastic regime in which the disease could be halted due to fluctuations or noise [15]. The disease reaches the final state when it stops spreading, and there are only susceptible and/or recovered nodes. In homogeneous networks with no community structure in the thermodynamic limit, the disease becomes an epidemic if a finite fraction of nodes is recovered, and it is an outbreak otherwise. In the SIR model, there exists a

---
*ldvaldez@bu.edu

critical value T_c below which the probability Π of an epidemic is null, while for $T > T_c$, $\Pi > 0$. However, note that not necessarily $\Pi = 1$ for $T > T_c$, so the disease could end up in an outbreak due to the fluctuations in the early dynamic, as mentioned above. Lagorio *et al.* [16] showed that there exists a cutoff s_c of the size of the number of recovered nodes above which the disease is in an epidemic state while below s_c it is an outbreak. Newman obtained that at the final state, the transmissibility T governs the fraction of recovered nodes which is identical to the relative size of the giant component (GC) for a link percolation process (with a probability of link occupation $p = T$) [14,17,18]. In turn, the SIR model exhibits a second-order transition at a critical threshold T_c which value coincides with the critical probability of link occupation in a link percolation process. The outcome of a disease does not depend only on the SIR parameters, β and t_r, but also on the network structure. Newman [14] showed that for a random homogeneous network (without communities) and having degree distribution $P(k)$ (where k is the connectivity or the number of neighbors of a node), the critical transmissibility T_c depends on the first moment $\langle k \rangle$, and second moment $\langle k^2 \rangle$ of the degree distribution. This is analogous to the percolation threshold found by Cohen *et al.* [19]. Kenah and Robins [20] generalized the results in Ref. [14] and found that the SIR maps with a semidirected link percolation process and their theory predicts the probability Π of an epidemic in the thermodynamic limit. Importantly, for a constant (homogeneous) recovery time, they proved that at the final state, the value of Π is equal to the relative size of the giant component of link percolation, P_∞. However, for the case of nonconstant (nonhomogeneous) recovery time and an infection time which follows an exponential distribution, $\Pi < P_\infty$ for $T > T_c$. This implies that the probability of an epidemic in the SIR model does not map to link percolation, i.e., this percolation process cannot predict the probability of an epidemic.

Several approaches have been developed to study the effects of the community structure on the disease spreading. Salathé *et al.* [21] found that in networks with a strong community structure, there exists a trapping effect because the disease is more likely to stay inside the community than to reach other communities. Besides, they obtained that such structure delays the epidemic spreading across the network. Hindes *et al.* [22] presented the time evolution equations in the thermodynamic limit for a network of subnetworks or communities in which at a global scale each community is represented by a "supernode," and all supernodes are arranged in a one-dimensional lattice, i.e., each supernode has only two supernode neighbors. They showed that if the disease starts in one of these communities, then the intradegree distribution affects the propagation front at a global scale. Vazquez [23] developed a model of communities composed by a finite number of nodes and solved it analytically. The author obtained that the disease spreading is characterized by oscillations at the early stages of the dynamic, and there exists a critical basic reproductive number (i.e., the number of secondary cases from an index case) above which the disease reaches a macroscopic number of communities. Colizza and Vespignani [24,25], and Barthelemy *et al.* [26] studied metapopulation systems or networks composed by subpopulations with

homogeneous mixing and homogeneous or heterogeneous degree between subpopulations over which individuals diffuse. For this model, they obtained deterministic reaction-diffusion equations that describe the disease spreading and found that there is a global invasion threshold, above which a pandemic emerges. They showed that this threshold depends on the degree heterogeneity and the number of individuals or agents moving among subpopulations. Recently, Sah *et al.* [27] studied on several realistic social networks of animals how the community structure affects disease spreading. The database included a wide range of structures ranging from quite homogeneous networks with a weak structure of communities to networks with highly segregated or fragmented communities such as raccoons, field voles, and northern elephant seals. The authors found, based on simulations, that the community structure does not affect the probability of epidemics or the fraction of infected nodes unless the global network has a very strong or extreme community structure. Finally, Nadini *et al.* [28] studied temporal networks with communities in which the number of nodes (size) in each community follows a power-law distribution. They found that in the limit of highly segregated communities, the final fraction of recovered nodes in the SIR model is reduced. Besides, in this limit, they obtained that when the community size is heterogeneous, the fraction of recovered nodes is higher than the case of a constant community size.

While many of the studies mentioned above analyzed the effect of communities on the disease spreading at a local and global scale, they are based only on simulations, or they do not consider the internal structure of the communities or subpopulations (such as in the case of metapopulation networks). A theoretical model that predicts the probability of a pandemic is still lacking in structured communities, that is, communities with an internal static structure.

In this paper, we develop a model and study it theoretically to understand the disease spreading at a global scale for the case of a static network with a strong community structure and find under which conditions a pandemic occurs. Additionally, we study how this structure shapes the evolution of the number of "infected" communities. Finally, in contrast to isolated networks [20], our work finds that link percolation predicts the probability of a pandemic due to the weak dependence of the global transmissibility (between communities) on their global recovery time.

II. MODEL

In this section, we explain the structure of the synthetic network with communities and the disease spreading process. In this work, we only consider static networks. Note that we describe our model at two scales: (1) a metalevel or global scale in which the communities are treated as supernodes and all the links between any two communities are represented by a single superlink, and (2) a microscopic or local scale in which the process is described at the level of the nodes and links in each community.

We consider a network of communities with a random structure in which the nodes of each community have internal connectivity or degree k that follows a distribution denoted as $P(k)$. The number of communities is N^g, and the number
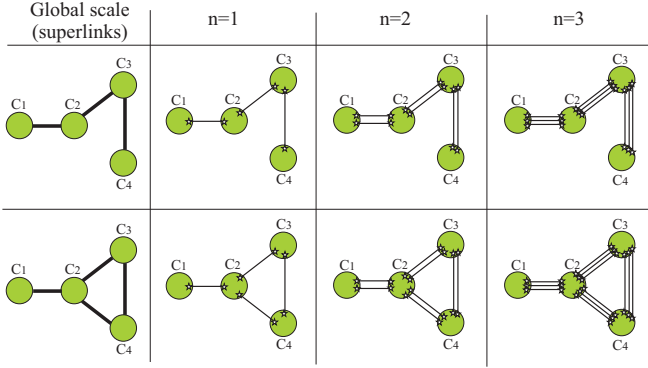
FIG. 1. Schematic illustration of four communities (C_1, C_2, C_3, and C_4, represented by circles) in which each row corresponds to a different global structure. The first column shows the global structure in which connections between communities are superlinks, and successive columns show different numbers of bridge nodes n (stars) for the same global structure: $n = 1$ (second column), $n = 2$ (third column), and $n = 3$ (fourth column). In all configurations for the first row C_2 and C_3 have two superlinks ($k^g = 2$), while C_1 and C_4 have only one ($k^g = 1$); for the second row C_1 has $k^g = 1$, and C_2, C_3, and C_4 have $k^g = 2$.
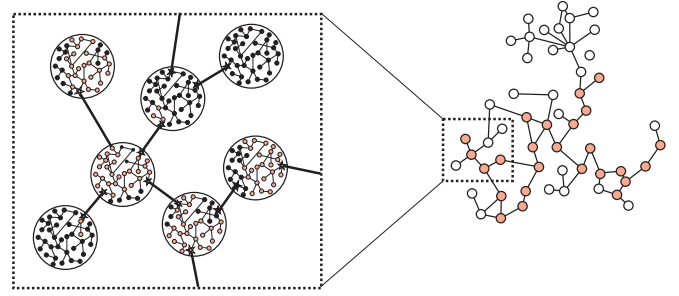

FIG. 2. Schematic illustration of the SIR model at the final state in a network with communities and $n = 1$. On the left, each large circle represents a community, stars denote bridge nodes, and small circles are the internal nodes or individuals of each community. The pink nodes correspond to recovered individuals, while the black ones are susceptible. On the right, we show the network of communities at a global scale where each circle is a supernode or community. The pink supernodes are the communities where the epidemic developed, and are white otherwise, i.e., the disease did not reach the community or only developed as an outbreak. The area enclosed with a dotted line corresponds to the figure on the left.

of nodes in each community is N_i with $i = 1, \ldots, N^g$. For simplicity, we assume that all the communities have the same internal degree distribution and the same number of nodes $N_i = N$ that could be either finite or infinite. The bridge nodes in one community are the nodes with external links, i.e., that are connected to other communities [29]. In our model, each bridge node always has only one link which connects to another community.

When $n = 1$, a community connects to another community only through one bridge node (see Fig. 1, second column). For $n > 1$, there are n bridge nodes of C_i that connect to n bridge nodes of C_j (see Fig. 1, third and fourth columns), where C_i and C_j denote the communities i and j, respectively. At a global scale, all these links between C_i and C_j are represented by a superlink, and we denote $P(k^g)$ as the fraction of communities or supernodes with k^g superlinks. Since a community with $k^g < \infty$ superlinks has $nk^g < \infty$ external links, in the limit $N \to \infty$ the number of external links for each community is insignificantly smaller compared to the number of its internal links. We refer to this structure or topology as an extreme or strong community structure because the number n of links between two communities is finite and insignificant compared to the number of links inside each community which is infinite in the thermodynamic limit. By increasing n we will show how a higher number of links among communities induces a pandemic. To study the disease spreading at a global scale from simulations, we consider that a community has an epidemic or a supernode is "infected" if its number of infected nodes or individuals is above a cutoff s_c, and susceptible if it is below s_c. Note that the value of s_c depends on the local degree distribution $P(k)$ of each community and its number of nodes (in Appendix A, we explain how to estimate s_c). The cutoff s_c allows distinguishing a macroscopic epidemic from a small outbreak. After a community or supernode is infected, it will go to the

"recovered" state when all the infected individuals within the community go to the recovered state.

Using this network as a substrate, we study a discrete-time SIR process. We define "microscopic transmissibility" T as the effective probability of infection between an infected node and its susceptible neighbor. At the microscopic level for the discrete-time dynamic, we consider that a node infects a susceptible neighbor with probability β per unit time step, and it recovers after t_r time steps. The microscopic transmissibility for this model is given by

$$T = 1 - (1 - \beta)^{t_r}. \qquad (1)$$

Here we will show the case of $t_r = 1$, in which case $T = \beta$, but qualitatively similar results are obtained for $t_r = 5$.

For the stochastic simulations in finite networks, at time $t = 0$, all the nodes of the whole network are susceptible except for one infected node or individual in a community chosen at random. In our dynamic model, we compute the temporal evolution of the fraction of infected supernodes and the fraction of recovered supernodes at the final state for a given value of T, which we denote as I^g and R^g, respectively. In finite networks, we consider that globally, the disease turns into a pandemic if the number of infected supernodes at the final state exceeds a threshold s_c. Note that at a global scale, the value of s_c depends on the global degree distribution $P(k^g)$ of supernodes. In this paper, since the local and global degree follow the same or similar degree distribution (for instance, a power-law distribution with similar exponent values at a local and global scale), we use the same value of s_c to distinguish outbreaks, epidemics, and pandemics (in Appendix A, we explain the method to estimate s_c based on simulations). On the other hand, in the thermodynamic limit ($N \to \infty$ and $N^g \to \infty$), a community or supernode has an epidemic if the fraction of recovered individuals is not zero, while a pandemic takes place if the fraction of recovered communities or supernodes is finite. Figure 2 shows a schematic illustration of the disease spreading at microscopic and global scales.

We define the "global transmissibility," T^g, as the effective probability of infection between an infected supernode and its susceptible supernode neighbor.

In the following sections, we present a mathematical approach to compute the global transmissibility and the relevant magnitudes that characterize the disease spreading at a global scale based on simulations and theory.

III. MICROSCOPIC AND MACROSCOPIC DYNAMIC

In this section, we study how the strong community structure affects the epidemic spreading dynamic at a microscopic and macroscopic scale. We denote an Erdős-Rényi network of Erdős-Rényi communities as ER-ER, that is, $P(k)$ and $P(k^g)$ follow a Poisson distribution, where k and k^g are the numbers of internal connectivities of a node and the number of superlinks of a supernode, respectively. Similarly, we denote a scale-free network of scale-free communities as SF-SF, where the degree distributions decay as a power law with exponent λ. It is important to note that the fraction of bridge nodes in any community is zero in the thermodynamic limit because they have $nk^g < \infty$ bridge nodes. The internal structure in each community is random, and at a global scale, the communities or supernodes are also randomly connected through the superlinks.

In the following, we show that the dynamic global spreading can be described by an SIR model in an aggregated network in which the supernodes do not have an internal structure, but they preserve the same degree distribution of superlinks $P(k^g)$ as in the model where supernodes are communities with internal structure. Analogously to the microscopic scale where the transmissibility is the probability that an infected node transmits the disease to its susceptible neighbor [given by Eq. (1)], in the aggregated network, we will obtain the global transmissibility T^g between an infected and susceptible supernodes. This magnitude will be computed from the probability of recovery time $P(\tau_R)$ and the distribution of infection time $P(\tau_I|\tau_R)$. Here τ_R is the time between two events in each community:

(i) the moment at which the number of infected nodes in the community is above s_c

(ii) the moment when no more infected nodes exist in the community after the first event took place.

The first event represents the fact that health authorities declare an epidemic only after having a certain number of infected individuals, and the second event represents the moment at which the authorities declare that the community is free of the epidemic.

Similarly, τ_I is the period in which a community A infects a community B (see schematic illustration in Fig. 3 of τ_I and τ_R). Using the above definitions of τ_I and τ_R, we define $T^g_{\tau_R}$ as the effective global transmissibility, which is the conditional probability that a supernode with recovery time τ_R infects its susceptible supernode neighbors and is given by:

$$T^g_{\tau_R} = \sum_{\tau_I=0}^{\tau_R} P(\tau_I|\tau_R), \qquad (2)$$

where $P(\tau_I|\tau_R)$ is the probability that a community A infects another B after τ_I time steps given that A recovers after τ_R time
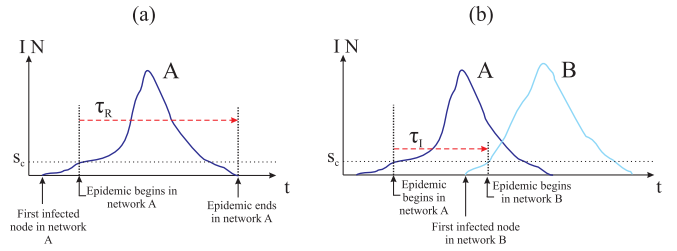

FIG. 3. Schematic illustration of the definition of τ_R (a) and τ_I when a community A infects B (b). The figures illustrate the time evolution of the number of infected nodes $I \times N$ in community A (dark blue) and community B (light blue). The horizontal dotted line corresponds to the threshold s_c above which a community is regarded as infected. In panel (a), the time τ_R (red dashed interval) corresponds to the time interval between the moment at which community A becomes infected, and the moment it recovers. In panel (b), the time τ_I (red dashed interval) corresponds to the time interval between the times in which the two communities A and B get infected.

steps. We also define the total effective global transmissibility T^g as

$$T^g = \sum_{\tau_R=0}^{\infty} T^g_{\tau_R} P(\tau_R), \qquad (3)$$

where $P(\tau_R)$ is the probability that a community recovers after τ_R time steps since it was infected.

From our simulations on communities that are not aggregated (they have internal structure), we obtain that the distribution of τ_R is broad, as shown in Fig. 4(a). Therefore, although at a microscopic level the recovery time of individuals or nodes is unique (t_r is the same for all nodes), the random
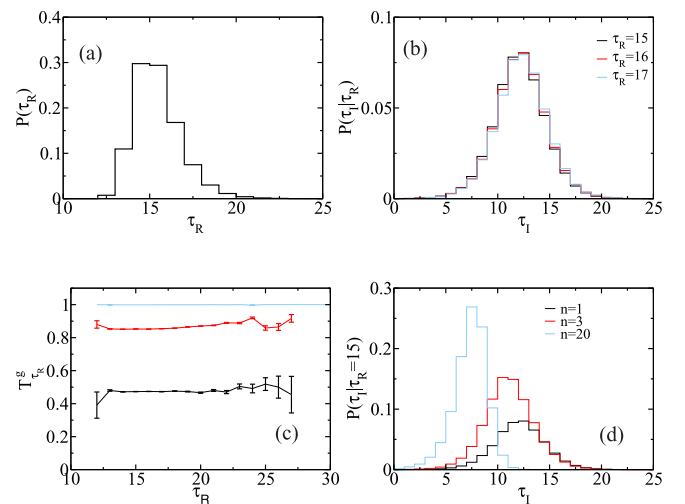

FIG. 4. Normalized time distribution of τ_R and τ_I for different values of n for two connected ER communities with $\langle k \rangle = 3$. (a) Distribution of τ_R. (b) The conditional distribution $P(\tau_I|\tau_R)$ for $n = 1$ and $\tau_R = 15$ (black), $\tau_R = 16$ (red), and $\tau_R = 17$ (light blue). (c) $T^g_{\tau_R}$ as a function of τ_R for $n = 1$ (black), $n = 3$ (red), and $n = 20$ (light blue). (d) The conditional distribution $P(\tau_I|\tau_R)$ for $\tau_R = 15$ and $n = 1$ (black), $n = 3$ (red), and $n = 20$ (light blue). The results were obtained with over 10^6 realizations for $T = 0.70$, $N = 10^4$, and $s_c = 100$.

internal structure of a community induces a distribution of recovery time at a global level. In Fig. 4(b), we show $P(\tau_I|\tau_R)$ for different values of τ_R in which we observe that increasing τ_R shifts slightly the probability $P(\tau_I|\tau_R)$ to the right (larger τ_I values).

Due to our definitions of infected and recovered communities at a global scale that are based on the cutoff s_c, we observe in Fig. 4(b) that for different values of recovery time τ_R, there is a range of values of τ_I in which $\tau_I > \tau_R$. This behavior implies that after a community A is declared free of the epidemic, A might infect a community B which seems to violate the causality of the spreading process because an already recovered community or supernode cannot infect another community or supernode. However, this case can occur since, at a microscopic scale before A recovers, its bridge nodes could transmit the disease to community B. However, since the number of infected nodes in B is still below s_c when A recovers, at a global scale B is susceptible, which explains the problem with causality. Nonetheless, because an increasing number of bridge nodes does not change $P(\tau_R)$, but moves to the left the distribution $P(\tau_I|\tau_R)$ [see Fig. 4(d)], the probability of $\tau_I > \tau_R$ decreases, thus the effect of lack of causality can be disregarded. On the other hand, this shift also implies that τ_I could be negative, but the probability of such an event is very low [$P(\tau_I < 0) \lesssim 10^{-4}$] for $n \leqslant 20$.

Using the recovery and infection time distribution shown in Figs. 4(a) and 4(b), we simulate a SIR model in a network with a degree distribution given by $P(k^g)$. We set $P(\tau_I|\tau_R) = 0$ for $\tau_I > \tau_R$ and for $\tau_I < 0$ to impose the causality.

In summary, to study the dynamic spreading for the aggregated network, we follow the next four steps:

(1) For a network with n bridge nodes, with N^g communities that follow a global degree distribution $P(k^g)$, and N nodes in each community that follows a local degree distribution $P(k)$, we built a network with N^g supernodes with the same degree distribution $P(k^g)$.

(2) Given (i) the values of the probability of infection β and the recovery time t_r, (ii) two communities with size N and local degree distribution $P(k)$, and (iii) these two communities have n bridge nodes, we run the SIR model and compute the time distributions $P(\tau_I|\tau_R)$ and $P(\tau_R)$.

(3) We run the SIR model in the aggregated network, using the distributions $P(\tau_I|\tau_R)$ and $P(\tau_R)$ as the infection time distribution between an infected and susceptible supernode, and the recovery time distribution of a supernode, respectively.

(4) We compute the fraction of infected supernodes I^g and compare to the fraction of infected communities in the microscopic network using the same values of β and t_r in step 2.

From Figs. 5(a) and 5(b), we observe that I^g obtained from the SIR in the aggregated network is in very good agreement with the results obtained from the SIR model on the network with communities, in particular, when the number of bridge nodes n increases. Similar results are also obtained for other values of T (see Appendix C), indicating that our model can be well described at a global scale as an SIR model. We also obtain that the area of I^g as a function of t is the same for different values of n (see insets in Fig. 5). In Appendix B, we show additional results on the effect of n on the average time $\langle t \rangle$ at which the fraction of infected communities is maximum.
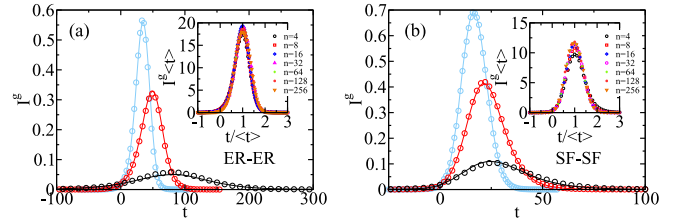

FIG. 5. Time evolution of the fraction of infected communities for different values of n: 1 (black), 3 (red), and 20 (light blue). For each value of n, we show the average value of I^g obtained from 100 realizations of the aggregated network (symbols) and the network with communities (line). Panel (a) corresponds to $T = 0.70$ for an ER network composed of ER communities with $\langle k^g \rangle = \langle k \rangle = 3$. Note that for $n = 1$, the disease reaches a macroscopic fraction of communities only for $T \gtrsim 0.6$ (see Fig. 7). Panel (b) corresponds to $T = 0.60$ for SF networks at a global scale with $\lambda = 3$ and $2 \leqslant k^g \leqslant 200$, with SF communities in which $\lambda = 2.5$ and $2 \leqslant k \leqslant 200$. For the simulations, we use $N = 10^4$, $N^g = 5 \times 10^3$, and $s_c = 100$. We set the time $t = 0$ as the moment at which $I^g N^g = s_c$ [30,31]. The insets show $I^g \langle t \rangle$ as a function of $t/\langle t \rangle$ for different values of n, where $\langle t \rangle$ is the time at which the fraction of infected communities is maximum. These results were obtained from the aggregated network.

In the following section and Appendix D 3, we show that the probability of a pandemic at the final state is well predicted by link percolation, although the distribution of recovery times is nonhomogeneous (which is in contrast with the results of Ref. [20]).

IV. FINAL STATE: GENERAL FORMALISM AND SIMULATIONS

A. Theory and critical point for a pandemic

Here we present the equations that describe the disease at the final state using percolation theory and the generating function formalism [32].

Assuming that $n = 1$, if community A develops an epidemic, then the effective or global probability of transmitting the epidemic to community B depends on the following events:

(i) a bridge node in a community A (that connects to community B) belongs to the GC of recovered nodes which size is above s_c. This event occurs with probability R.

(ii) an infected bridge node transmits the disease to the bridge node in community B with probability T [see Eq. (1)].

(iii) the disease in community B becomes an epidemic (i.e., $R > 0$ in community B) with probability Π.

At a global scale, the effective or global probability of infection from one community to another is $TR\Pi$. Similarly, for the case of $n > 1$ bridges, the effective probability of transmission is

$$1 - (1 - TR\Pi)^n \equiv T^g. \tag{4}$$

which is the probability that at least one bridge node in community A transmits the disease to a bridge node in community B from which an epidemic develops. Note that R and Π are magnitudes relative to one community which depend on the microscopic transmissibility T, and they are evaluated based on Ref. [20] (see a brief explanation in Appendix D). For the

case of a fixed or homogeneous recovery time, $\Pi = R$ [20] which are obtained solving the following equations:

$$f_\infty = 1 - G_1(1 - Tf_\infty), \tag{5}$$

$$R = 1 - G_0(1 - Tf_\infty), \tag{6}$$

where f_∞ is the probability that a link leads to a macroscopic recovered cluster of nodes in a branching process, and $G_0(x)$ and $G_1(x)$ are the generating functions of the degree distribution and the excess degree distribution of a node, respectively [14,33].

Using the effective global transmissibility T^g, we compute the fraction of recovered communities or supernodes R^g at the final state. This magnitude is obtained from two generating functions that describe the network structure at a global scale, and are given by

$$G_0^g(x) = \sum_{k^g=0}^\infty P(k^g)x^{k^g}, \tag{7}$$

$$G_1^g(x) = \sum_{k^g=0}^\infty \frac{k^g P(k^g)}{\langle k^g \rangle} x^{k^g-1}. \tag{8}$$

With these generating functions $G_0^g(x)$ and $G_1^g(x)$, considering the aggregated system as a single network in which nodes do not have any internal structure, the equations of the SIR model at the final state are given by

$$f_\infty^g = 1 - G_1^g(1 - T^g f_\infty^g), \tag{9}$$

$$R^g = 1 - G_0^g(1 - T^g f_\infty^g), \tag{10}$$

where T^g is the effective transmissibility between communities [see Eq. (4)], R^g is the fraction of recovered communities, and f_∞^g is the probability that a superlink leads to a macroscopic recovered cluster of supernodes in a branching process [14,33]. Note that Eqs. (9) and (10) are the same as the SIR model in a network without communities [14,33] for a transmissibility T^g. However, we are interested in understanding how the microscopic transmissibility T affects the order parameter R^g for a pandemic [replacing Eq. (4) in Eqs. (9) and (10)] [34].

Applying the technique used in Refs. [14,33] to find the critical point, and using that $R = \Pi$ for a homogeneous recovery distribution, we obtain from Eq. (9) and Eqs. (5) and (6) that for ER-ER networks, the critical microscopic transmissibility of a pandemic $T_{c,\text{pand}}$ (above which $f_\infty^g > 0$, that is, $R^g > 0$) satisfies the following equation

$$1 - \left(\frac{\Delta}{T_{c,\text{pand}}}\right)^{1/2} = e^{-\langle k \rangle (T_{c,\text{pand}}\Delta)^{1/2}}, \tag{11}$$

where $\Delta \equiv 1 - (1 - 1/\langle k^g \rangle)^{1/n}$, $\langle k^g \rangle$ is the mean number of the superlinks of each supernode, and $\langle k \rangle$ is the mean connectivity inside each community. Note that $T_{c,\text{pand}}$ depends on the number of bridge nodes n, similar to the metapopulation networks [24–26] where the global invasion threshold depends on the number of individuals or agents moving among subpopulations.

From Eq. (11), we obtain that $T_{c,\text{pand}} \to 1$ as $\langle k \rangle$ and $\langle k^g \rangle$ decrease because in this limit a pandemic only develops
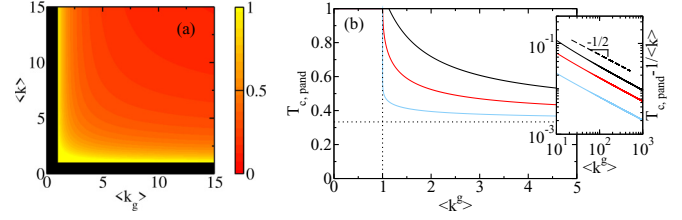

FIG. 6. (a) Heat-map of the critical microscopic transmissibility for a pandemic, $T_{c,\text{pand}}$, in the plane $\langle k^g \rangle$ and $\langle k \rangle$ for an ER network of ER communities and $n = 1$. The black region indicates that there is no pandemic phase in the network for any value of the microscopic transmissibility. (b) Critical microscopic transmissibility for a pandemic $T_{c,\text{pand}}$ as a function of the global mean degree $\langle k^g \rangle$ for ER network of ER communities with $\langle k \rangle = 3$ and different values of n: 1 (black), 3 (red), and 20 (light blue). For each value of n, the system is in a pandemic phase above the curves, while below it is free of a pandemic. The vertical dotted line indicates the limit $\langle k^g \rangle = 1$ and the horizontal dotted line corresponds to $T_{c,\text{pand}} = T_c = 1/\langle k \rangle$. The inset shows $T_{c,\text{pand}} - 1/\langle k \rangle$ as a function of $\langle k^g \rangle$ in log-log scale for the curves shown in the main plot. The curves and the surface are obtained from Eq. (11). Note that the slope $= -1/2$ is predicted in Eq. (12).

at the highest probability of transmission to overcome the sparseness at a local and global scale [35] [see Fig. 6(a)]. On the other hand, as $\langle k^g \rangle$ increases for a fixed value of $\langle k \rangle$, $T_{c,\text{pand}}$ converges as a power-law to the critical value of an isolated community $T_c = 1/\langle k \rangle$ [see inset of Fig. 6(b)]. Expanding Eq. (11) for $\langle k^g \rangle \gg 1$, we obtain that $T_{c,\text{pand}}$ behaves as

$$T_{c,\text{pand}} \approx \frac{1}{\langle k \rangle} + \frac{1}{2}\left(\frac{1}{n\langle k^g \rangle \langle k \rangle}\right)^{1/2}. \tag{12}$$

From Eq. (12) we can see that $T_{c,\text{pand}}$ decreases with the number of bridge nodes as a power law, and for $n \to \infty$, $T_{c,\text{pand}} \to T_c = 1/\langle k \rangle$. Note that after an epidemic develops in one community, the probability that the disease reaches one bridge node increases with n. In turn, the probability that at least one of the infected bridge node induces an epidemic in a susceptible community also increases with n. As a consequence, for large n, the disease cannot be confined in one community, and the fluctuations of the early dynamic that extinguish the disease in a community cannot "halt" the disease spreading at a global scale. Therefore, in the limit $n \to \infty$ at the final state, $T_c = T_{c,\text{pand}}$, and there is no distinction between the outcome of an epidemic and pandemic since one implies the other [see Eq. (12)].

B. Size and probability of a pandemic

Besides the computation of the critical transmissibility for a pandemic, it is also of interest to study the size of the pandemic in terms of the number of recovered individuals and communities with epidemics.

In Fig. 7, we show the fraction of recovered individuals R^{tot} in the whole system and the fraction of communities that developed an epidemic at the final state R^g (where $R^{\text{tot}} \equiv R^g R$) obtained from Eqs. (9) and (10) and simulations. For ER-ER and SF-SF networks with $n = 1$, there is little difference between R^{tot} and R^g because the degree distributions at a
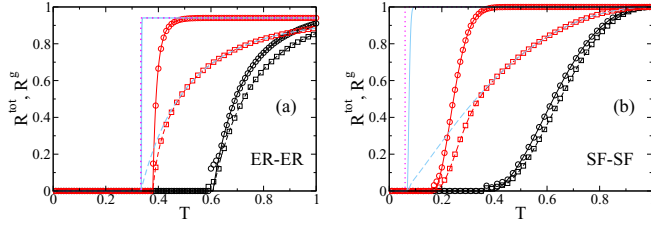
FIG. 7. Fraction of recovered individuals R^{tot} ($\square$, dashed line) and communities that developed an epidemic R^g ($\bigcirc$, solid line) as a function of the microscopic transmissibility. Our results were obtained from the simulations (symbols) and Eqs. (9) and (10) (lines) for $n = 1$ (black), $n = 20$ (red), and $n = 10^4$ (light blue, only theory). The pink dotted line corresponds to the limit $n = \infty$ [see Eq. (13)]. Panel (a) corresponds to an ER network of ER communities with $\langle k^g \rangle = \langle k \rangle = 3$. Panel (b) corresponds to SF networks at a global scale with $\lambda = 3$ and $2 \leqslant k^g \leqslant 200$, with SF communities in which $\lambda = 2.5$ and $2 \leqslant k \leqslant 200$. The simulations were performed over 100 network realizations with $N = 10^4$, $N^g = 5 \times 10^3$, and (a) $s_c = 600$ and (b) $s_c = 100$.

local $[P(k)]$ and global $[P(k^g)]$ scales are similar, and $T^g \not\approx 1$ for $n = 1$ [see Eq. (4)]. However, as the number of bridge nodes increases, the curves R^{tot} and R^g differ from each other, particularly close to the critical point.

It is interesting to note that the fraction of recovered individuals R^{tot} converges to a function that vanishes continuously at $T_{c,\text{pand}}$, in contrast to the fraction of recovered communities R^g that converges to a discontinuous step function for $n \to \infty$:

$$R^g(T, n = \infty) = \begin{cases} c & \text{if } T > T_{c,\text{pand}} = T_c \\ 0 & \text{if } T \leqslant T_{c,\text{pand}} = T_c \end{cases}, \quad (13)$$

where $c > 0$ and constant. This is because for any value of the microscopic transmissibility $T > T_c$ when $n \to \infty$, the global transmissibility tends to $T^g \to 1$ [see Eq. (4)]. In consequence, if the epidemic begins in a community or supernode that belongs to the GC of supernodes, the disease will reach all the supernodes that belong to this cluster for any value of $T > T_c$. The value of $R^g(T, n = \infty)$ is a constant and corresponds to the fraction of supernodes that belong to the GC at a global scale. On the other hand, for $T < T_c$ the disease never becomes an epidemic in a community and hence it cannot becomes a pandemic which implies that $R^g(T, n = \infty) = 0$.

For the case $n = 1$, the size of a pandemic is comparable (or correlated) to the size of an epidemic in each community. In such a scenario, if the authorities decide to apply a strong mitigation strategy to prevent the disease spreading when the fraction of infected communities is large, this also corresponds to a significant fraction of infected individuals in each community. However, if the number of bridge nodes n increases, any strong response measure to halt an extended global disease could be considered "disproportionate" if the size of the epidemic in each community is small, especially near the critical point. The increasing distance between the curves R^{tot} and R^g as n increases, establishes a problematic scenario to any strategy that is based only on the number of infected communities because if it is declared that a disease has reached a pandemic status, it may be thought as alarmist
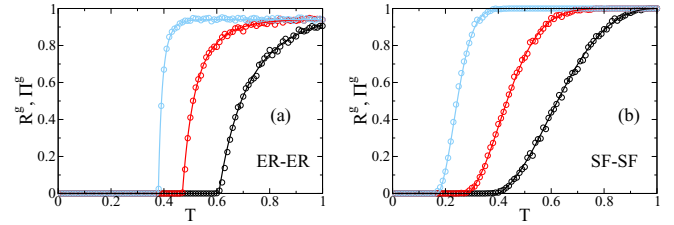

FIG. 8. Probability of a pandemic given that there is one community with an epidemic as a function of T for $n = 1$ (black), $n = 3$ (red), $n = 20$ (light blue). Panel (a): The results correspond to an ER network of ER communities with $\langle k^g \rangle = \langle k \rangle = 3$, and different values of n. Panel (b) corresponds to SF networks at a global scale with $\lambda = 3$ and $2 \leqslant k^g \leqslant 200$, with SF communities in which $\lambda = 2.5$ and $2 \leqslant k \leqslant 200$. The simulations were performed over 10^3 network realizations with $N = 10^4$, $N^g = 5 \times 10^3$, and (a) $s_c = 600$ and (b) $s_c = 100$. The lines (R^g) correspond to the theory obtained from the Eqs. (9) and (10), and the symbols (Π^g) to the simulations.

since $R^{\text{tot}} \ll R^g$. Therefore, this result suggests that the size of the epidemic in each community could also be used to decide the required aggressiveness of the mitigation strategy since this would allow identifying pandemics that do not affect a substantial fraction of the population near $T_c = T_{c,\text{pand}}$.

Another significant concern for health authorities is the probability of a false-positive pandemic alert because a false alarm would also induce mistrust, panic, and fear in the population. In Figs. 8(a) and 8(b), we show the probability Π^g that the disease develops into a pandemic, given that there is at least one community with an epidemic. Remarkably, we observe that this probability is very close to the fraction of recovered communities at the final state, i.e., $R^g \approx \Pi^g$, despite that the time recovery distribution $P(\tau_R)$ is nonhomogeneous [see Fig. 4(a)]. This relation holds because the transmissibility $T^g_{\tau_R}$ has a weak dependence on τ_R [see Fig. 4(c)]. In fact, in Appendix D 3, we show based on a simple model that the SIR model with nonhomogeneous recovery time and constant $T^g_{\tau_R}$ maps into link percolation, i.e., $R = \Pi$. Therefore our results in Fig. 4(c) and Appendix D 3 suggest that $R^g \approx \Pi^g$ in a network with communities, and hence the probability of a pandemic converges to the step function given in Eq. (13). Thus, after a community develops an epidemic, not only a large number of communities would develop epidemics (close to 100%) if no intervention from any authority is implemented, but also, it is very likely to declare a pandemic. Besides, this implies that in a more interconnected world and near the critical point, it is very likely that health authorities will face a scenario in which the disease reaches many regions (communities) with a small fraction of infected individuals.

V. SUMMARY AND CONCLUSIONS

In summary, we have studied the effect of extreme modularity in structural modular networks on disease spreading at a global scale. We found that the epidemic spreading through the network at a global scale can be described as an SIR model with renormalized infection and recovery distributions. On the other hand, as n increases, the probability and size of a pandemic increase and tend to a discontinuous function of the

transmissibility after the disease has reached the status of the epidemic in one community. Besides, if the transmissibility T is close to the critical value of an epidemic, our results indicate that the fraction of recovered communities is significantly higher than the fraction of recovered individuals. This situation can lead to a scenario in which a pandemic alarm could be considered as an excessive alarm causing fear in the global population. Finally, our simulations show that link percolation is a good approximation to describe the final state of the disease spreading at a global scale in random networks, although the recovery time distribution of a community is nonhomogeneous.

An important simplification of our work is that all communities have the same degree distribution and the same number of nodes N and bridge nodes n. Our future studies will consider a distribution on these magnitudes among the communities to explore how they affect the size and probability of a pandemic.

APPENDIX A: THRESHOLD s_c

In the simulations of the SIR model, fluctuations due to stochasticity could lead that the number of infected nodes vanishes fast after the disease spreading started and the number of recovered nodes is very small compared to the size of the system, even for high values of transmissibility close to $T = 1$. Lagorio *et al.* [16] proposed a method to distinguish an outbreak from an epidemic, computing the distribution of final sizes $P(s)$ of the disease from the simulations of the SIR model. For $T > T_c$, $P(s)$ has a bimodal behavior, as shown in Fig. 9. The left side of the distribution corresponds to outbreaks, while the peak on the right corresponds to epidemics. Between these two regions, there is a gap in which the probability $P(s)$ is null. Therefore, any value of the threshold s_c that belongs to this region can be used to distinguish epidemics and outbreaks. In Figs. 9(a) and 9(b), we observe that as the transmissibility T approaches T_c from above, that gap mentioned above shrinks, and the distribution corresponding to outbreaks becomes broader, and hence the minimum possible value of s_c increases.

From the distributions $P(s)$ in Figs. 9(a) and 9(b), we estimate the values of s_c that we use in this research. In the main text, Sec. III we choose $s_c = 100$ for ER networks with $\langle k \rangle = 3$ and $T = 0.7$, and $s_c = 100$ for SF networks at $T = 0.60$, since this threshold distinguish outbreaks and
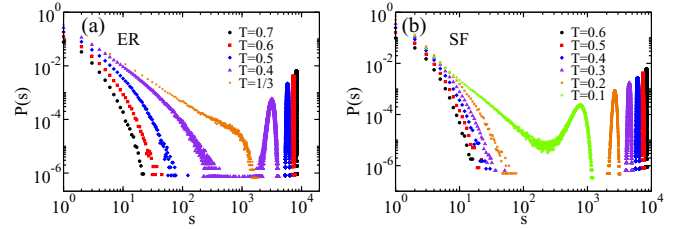

FIG. 9. Distribution of the number of recovered nodes at the final state, $P(s)$ for different values of T for networks without community structure. Panel (a) corresponds to an ER network with $\langle k \rangle = 3$. Panel (b) corresponds to a SF network with $\lambda = 2.5$, $k_{\min} = 2$, and $k_{\max} = 200$. The simulations results were averaged over 10^6 network realizations with $N = 10^4$.

epidemics. On the other hand, to explore the size and probability of a pandemic for different values of T, we set:

(i) $s_c = 600$ for ER networks with $\langle k \rangle = 3$ which is a sufficient threshold to distinguish epidemic for $T > 0.4$. Note that $T_c = 1/3$.

(ii) $s_c = 100$ for SF networks, which is a sufficient threshold to distinguish an epidemic for $T > 0.2$.

APPENDIX B: RESULTS FOR DIFFERENT VALUES OF T AND n

In Fig. 10 we show the time $\langle t \rangle$ at which I^g is maximum as a function of n for different topologies and values of the transmissibility. We observe that for large values of n, $\langle t \rangle$
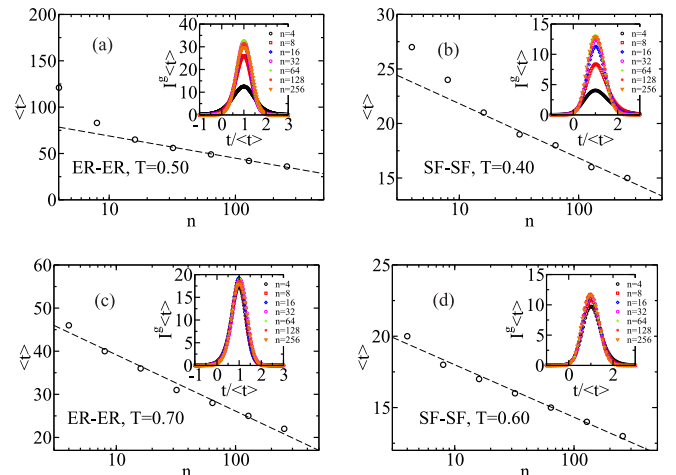

FIG. 10. The time $\langle t \rangle$ at which the fraction of infected communities is maximum, as a function of n in linear-log scale. Panels (a) and (c) correspond to $T = 0.50$ and $T = 0.70$, respectively, for an ER network of ER communities with $\langle k^g \rangle = \langle k \rangle = 3$. Panels (b) and (d) correspond to $T = 0.40$ and $T = 0.60$, respectively, for SF networks at a global scale with $\lambda = 3$ and $2 \leqslant k^g \leqslant 200$, with SF communities in which $\lambda = 2.5$ and $2 \leqslant k \leqslant 200$. The dashed line corresponds to a logarithmic fit $\langle t \rangle = A + B \ln(n)$, where $A = 92.8$ and $B = -10.4$ (a), $A = 26.4$ and $B = -2.16$ (b), $A = 52.2$ and $B = -5.7$ (c), and $A = 21.7$ and $B = -1.6$ (d). For the simulations, we use $N = 10^4$, $N^g = 5 \times 10^3$, and $s_c = 100$. We set the time $t = 0$ as the moment at which $I^g N^g = s_c$. The insets show $I^g \langle t \rangle$ as a function of $t/\langle t \rangle$ for different values of n.
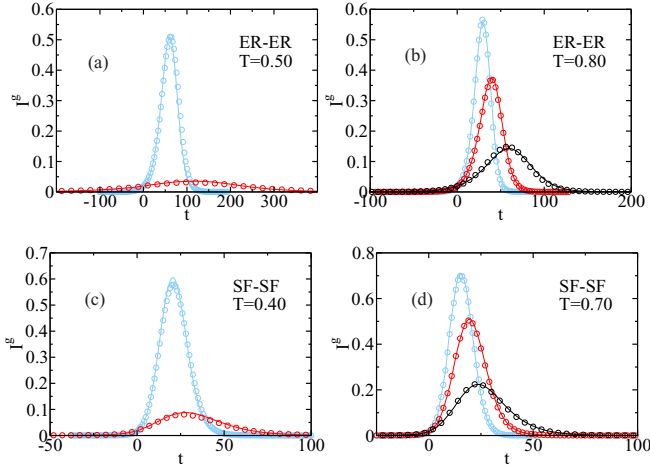
FIG. 11. Time evolution of the fraction of infected communities for different values of n: 1 (black), 3 (red), and 20 (light blue). Other parameters are the same as in Figs. 5(a) and 5(b). For each value of n, we show the average value of I^g obtained from 100 realizations of the aggregated network (symbols) and the network with communities (line). Note that for panels (a) and (c), we do not show I^g for $n = 1$ because, in that case, the transmissibility is close or below $T_{c,\mathrm{pand}}$ [see Figs. 7(a) and 7(b)].

behaves as a logarithm function. Besides, we obtain that the area of I^g as a function of t converges to the same value as n increases (see insets in Fig. 10).

APPENDIX C: MACROSCOPIC DYNAMIC: ADDITIONAL RESULTS

In Figs. 11(a) and 11(b), similar to Figs. 5(a) and 5(b), we show the time evolution of I^g obtained from the aggregated network and from the microscopic model for other values of transmissibility T. In all cases, we observe an agreement between the results for the aggregated network and the microscopic model.

APPENDIX D: PERCOLATION IN SEMIDIRECTED NETWORKS AND THE SIR MODEL

In this Appendix, we review Refs. [20,36] in the first two sections, which showed the mapping between SIR and a percolation process in a semidirected network. In the third section, we develop a simple model which shows that the SIR model with nonhomogeneous recovery time maps into link percolation if $T_{\tau_R}^g$ is constant.

1. Method

The key idea to study the final state of the SIR model using percolation theory is to consider that there is a mapping between the set of realizations of the stochastic SIR simulations and a percolation process in a semidirected network. To see this mapping, let us consider that during the stochastic simulation of the SIR model, node i is infected at time t. Immediately after that, the algorithm of the simulation generates a random recovery time τ_R obtained from a probability distribution $P(\tau_R)$. Hence, node i will recover at time $t + \tau_R$.

Similarly as in the Gillespie algorithm, for each neighbor of i, a random time τ_I is generated following a distribution $P(\tau_I|\tau_R)$ in which node i transmits the disease (since the moment that i was infected).

Alternatively, instead of this procedure generating random numbers "on the fly," i.e., during the simulation of the dynamic process, the random numbers τ_R and τ_I can be obtained before starting the dynamic. More specifically, a recovery time τ_R is generated from a distribution $P(\tau_R)$ for each node before an index case appears in the network. Note that the generation of τ_R does not guarantee that a node i will be infected, but in case node i gets infected during the dynamic process (that we explained below), it would recover after a period τ_R. After we obtain the value of τ_R for a node i, we generate the times the disease will take to reach each neighbor j of i, including the possibility that $\tau_I = \infty$, in which case, node i will never infect node j. Each link from i with $\tau_I < \infty$ is represented by an occupied arrow from i to the other node connected through this link. Analogously to the case of the recovery time, an arrow from i to j does not mean that i will effectively infect j, but in case i gets infected at time t during the dynamic, then j would be infected at time $t + \tau_I$ (if another node does not infect j before this time).

The process described above does not develop the dynamic but only generates all random numbers τ_R and τ_I before starting the dynamic. In the case where two nodes point to each other, their link is occupied and undirected, and if there is no arrow between these nodes, their link is unoccupied. As a result of this procedure, we obtain a semidirected network.

After assigning all the times τ_R and τ_I, a random node is chosen as the index case, and then, the dynamic of the disease spreading consists in following the arrows that emerge from the index case, as described in Refs. [20,36]. If another node is chosen as the index case, then the branch of infection would be different, so the semidirected network contains many realizations of the SIR model. Although this process is an alternative approach to "on the fly" algorithm, it also allows interpreting many realizations of the SIR model as a semidirected network. We will see below that this interpretation is useful for calculating the probability of an epidemic Π and the fraction of recovered nodes R at the final state.

2. Relationship between the in-component and out-component with R and Π

In this section, we introduce several definitions of semidirected networks and then their relation to the fraction of recovered nodes and the probability of an epidemic.

In any semidirected network, each node i has three types of degree or connections:

(i) indegree: the number of incoming links to i,

(ii) outdegree: the number of outgoing links from i,

(iii) undirected degree: the number of undirected links of i.

The generating function of the probability p_{abc} that a node has indegree "a," outdegree "b," and undirected degree "c" is given by

$$G_0(x, y, u) = \sum_{a=0}^{\infty} \sum_{b=0}^{\infty} \sum_{c=0}^{\infty} p_{abc} x^a y^b u^c. \qquad (D1)$$

The mean indegree $\langle k_{\text{in}} \rangle$, outdegree $\langle k_{\text{out}} \rangle$, and undirected degree $\langle k_u \rangle$ are

$$\langle k_{\text{in}} \rangle = \frac{\partial G_0}{\partial x}(1,1,1) = \sum_{a=0}^{\infty} \sum_{b=0}^{\infty} \sum_{c=0}^{\infty} a \, p_{abc}, \quad \text{(D2)}$$

$$\langle k_{\text{out}} \rangle = \frac{\partial G_0}{\partial y}(1,1,1) = \sum_{a=0}^{\infty} \sum_{b=0}^{\infty} \sum_{c=0}^{\infty} b \, p_{abc}, \quad \text{(D3)}$$

$$\langle k_u \rangle = \frac{\partial G_0}{\partial u}(1,1,1) = \sum_{a=0}^{\infty} \sum_{b=0}^{\infty} \sum_{c=0}^{\infty} c \, p_{abc}. \quad \text{(D4)}$$

Since the total number of incoming connections is the same as the total number of outgoing connections, then $\langle k_{\text{in}} \rangle = \langle k_{\text{out}} \rangle \equiv \langle k_d \rangle$.

In a branching process, if we choose a node through a directed link following its direction (forward), a directed link going in the opposite direction (reverse or backward), or through a link without direction (undirected), then the generating functions that the reached node has indegree "a," outdegree "b," and undirected degree "c" are given by

$$G_f(x,y,u) = \frac{1}{\langle k_d \rangle} \frac{\partial G_0}{\partial x}(x,y,u), \quad \text{(D5)}$$

$$G_r(x,y,u) = \frac{1}{\langle k_d \rangle} \frac{\partial G_0}{\partial y}(x,y,u), \quad \text{(D6)}$$

$$G_u(x,y,u) = \frac{1}{\langle k_u \rangle} \frac{\partial G_0}{\partial u}(x,y,u), \quad \text{(D7)}$$

respectively.

Following the definitions of Ref. [32], in semidirected networks, there exist for each node i an:

(i) in-component that is the set of nodes from which i can be reached by following the arrows. We define this component as macroscopic in-component ($\mathcal{M}_{\text{in}}$) if the number of nodes of this set is macroscopic. Otherwise, it belongs to a finite in-component.

(ii) out-component that is the set of nodes that can be reached from i following the arrows. We define this component as macroscopic out-component ($\mathcal{M}_{\text{out}}$) if the number of nodes of this set is macroscopic. Otherwise, it belongs to a finite out-component.

For a randomly chosen node, the generating functions of the *finite* sizes of its in-component and out-component are denoted by $H^{\text{in}}(z)$ and $H^{\text{out}}(z)$, respectively. These generating functions can be obtained using a backward and forward branching, that is, following the arrows in the opposite and along to their directions, respectively. Note that in this branching process, it is assumed that the network is in the thermodynamic limit ($N \to \infty$) and the structure is random. For a backward branching process, the generating functions of the size of an in-component corresponding to a randomly chosen node through a link, are

(i) $H_r^{\text{in}}(z)$ if the node is reached when going in the opposite direction of an arrow [see Fig. 12(a)]

(ii) $H_u^{\text{in}}(z)$ if the node is reached through an undirected link.

Note that we do not consider $H_f^{\text{in}}(z)$, i.e., when a node is reached following the direction of an arrow because, in this case, the branching process would not correspond to an in-component. Analogously, for a forward branching process,
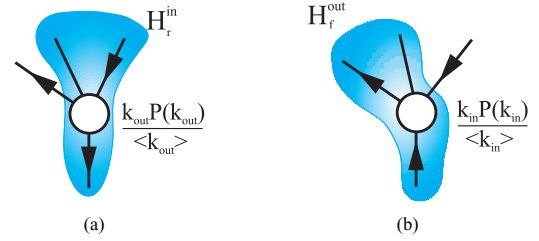

FIG. 12. Schematic figure of the backward (a) and forward branching (b). The direction of the branching process goes from bottom to top. Solid lines without any arrow represent undirected links, and arrows represent links with a direction. The blue area depicts the set of links used in the backward branching (a) and forward branching (b). For a backward (forward) branching, a node is reached through one of its outgoing (incoming) links with probability $k_{\text{out}} P(k_{\text{out}})/\langle k_{\text{out}} \rangle$ [$k_{\text{in}} P(k_{\text{in}})/\langle k_{\text{in}} \rangle$] and the in-component (out-component) continue to grow through its incoming (outgoing) and undirected links.

the generating functions of the size of an out-component corresponding to a randomly chosen node through a link, are

(i) $H_f^{\text{out}}(z)$ if the node is reached going in the same direction of an arrow [see Fig. 12(b)]

(ii) $H_u^{\text{out}}(z)$ if the node is reached through an undirected link.

For the case of a semidirected network constructed by the procedure explained in the previous section, if the index case has a finite out-component, the disease can only reach a finite number of nodes following the arrows. Therefore, the probability that an index case does not trigger an epidemic, $1 - \Pi$, is equal to the probability that it belongs to a finite out-component $H^{\text{out}}(1)$. Otherwise, if the index case belongs to the $\mathcal{M}_{\text{out}}$, this realization of the SIR model corresponds to an epidemic. Besides, Ref. [20] also showed that using the same semidirected network, the fraction of recovered nodes R is equal to the probability that a node belongs to an $\mathcal{M}_{\text{in}}$ [$R = 1 - H^{\text{in}}(1)$]. To see this, let us assume that there is an infinitesimal but not null fraction ϵ of infected nodes during the dynamic spreading in the semidirected network, in which case there is an epidemic (i.e., $R \geqslant \epsilon > 0$) [37]. In the case for any susceptible node i that has an $\mathcal{M}_{\text{in}}$, at least one of the nodes in its $\mathcal{M}_{\text{in}}$ will be infected in the thermodynamic limit (with probability 1). Consequently, the disease will reach node i following the arrows of the semidirected network. However, if a susceptible node i has a finite in-component in which all of its nodes are susceptible, then i will never be reached by the disease. In turn, the probability that at least one of the nodes of this finite in-component is infected, vanishes as $\epsilon \to 0$, and hence the disease can only reach the nodes within a $\mathcal{M}_{\text{in}}$. Therefore, when there is an epidemic, the fraction of nodes within a $\mathcal{M}_{\text{in}}$ is equal to the fraction of recovered nodes R at the final state.

In the following, we present the explicit relation between the generating functions of the degree of a semidirected network and the SIR model described in Sec. D 1.

For a node i with a recovery time τ_R [with probability $P(\tau_R)$], the probability that each connection is as follows:

(i) occupied and outgoing is $T_{\tau_R}(1 - T)$, i.e., node i points its neighbor, but its neighbor does not point to i,

TABLE I. Distribution $P(\tau_I|\tau_R)$ for T_{τ_R} constant.

	$\tau_I = \infty$	$\tau_I = 1$	$\tau_I = 2$	$\tau_I = 10$
$\tau_R = 2$	$1 - \sigma$	0.5σ	0.5σ	0
$\tau_R = 10$	$1 - \sigma$	0.5σ	0	0.5σ

TABLE II. Distribution $P(\tau_I|\tau_R)$ for nonhomogeneous T_{τ_R}.

	$\tau_I = \infty$	$\tau_I = 1$	$\tau_I = 2$	$\tau_I = 10$
$\tau_R = 2$	$1 - \sigma^{10}$	$0.5\sigma^{10}$	$0.5\sigma^{10}$	0
$\tau_R = 10$	$1 - \sigma$	0.5σ	0	0.5σ

(ii) occupied and incoming is $(1 - T_{\tau_R})T$, i.e., i does not point to its neighbor, but its neighbor points i,

(iii) occupied and undirected is $T_{\tau_R}T$,

(iv) unoccupied is $(1 - T_{\tau_R})(1 - T)$,

where $T_{\tau_R} = \sum_{\tau_I=0}^{\tau_R} P(\tau_I|\tau_R)$ is the transmissibility given that node i has recovery time τ_R, and $T = \sum_{\tau_R=0}^{\infty} T_{\tau_R} P(\tau_R)$ is the total transmissibility.

Since the generating function of the total degree of a node is $G_0(z) = \sum P(k)z^k$, then the generating function of the probability p_{abc} that a node has indegree "a," outdegree "b," and undirected degree "c" [see Eq. (D1)] can be rewritten as

$$G_0(x, y, u) = \sum_{k=0}^{\infty} P(k) \sum_{\tau_R=0}^{\infty} P(\tau_R)$$
$$\times \left[(1 - T_{\tau_R})(1 - T) + (1 - T_{\tau_R})Tx \right.$$
$$\left. + T_{\tau_R}(1 - T)y + T_{\tau_R}Tu \right]^k. \quad \text{(D8)}$$

Following Ref. [20], the generating function $H^{\text{out}}(z)$ is obtained from the following equations:

$$H_f^{\text{out}}(z) = zG_f\big(1, H_f^{\text{out}}(z), H_u^{\text{out}}(z)\big), \quad \text{(D9)}$$

$$H_u^{\text{out}}(z) = zG_u\big(1, H_f^{\text{out}}(z), H_u^{\text{out}}(z)\big), \quad \text{(D10)}$$

$$H^{\text{out}}(z) = zG_0\big(1, H_f^{\text{out}}(z), H_u^{\text{out}}(z)\big). \quad \text{(D11)}$$

For the case of homogeneous recovery time (τ_R is constant), these equations are reduced to those proposed by Newman [14] using an analogy between the SIR model and link percolation:

$$f_\infty = 1 - G_1(1 - T f_\infty), \quad \text{(D12)}$$

$$R = 1 - G_0(1 - T f_\infty). \quad \text{(D13)}$$

where f_∞ is the probability that a link leads to a macroscopic recovered cluster of nodes in a branching process [14,33].

On the other hand, the generating function $H^{\text{in}}(z)$ is obtained from the following equations:

$$H_r^{\text{in}}(z) = zG_r\big(H_r^{\text{in}}(z), 1, H_u^{\text{in}}(z)\big), \quad \text{(D14)}$$

$$H_u^{\text{in}}(z) = zG_u\big(H_r^{\text{in}}(z), 1, H_u^{\text{in}}(z)\big), \quad \text{(D15)}$$

$$H^{\text{in}}(z) = zG_0\big(H_r^{\text{in}}(z), 1, H_u^{\text{in}}(z)\big). \quad \text{(D16)}$$

Reference [20] showed that $\Pi = 1 - H^{\text{out}}(1) \leqslant R = 1 - H^{\text{in}}(1)$, and hence the SIR does not map with link percolation because this percolation process implies that $\Pi = R$. However, it was shown in Ref. [20] that for the case in which the recovery time is constant, forward and backward branching are equivalent and consequently $R = \Pi$.

3. Nonhomogeneous recovery time with homogeneous transmissibility

In Ref. [20], the authors presented the main ideas and equations to solve the SIR model with any recovery time τ_R distribution and an infection time τ_I that follows an exponential distribution. They showed that for any recovery time distribution, $\Pi \leqslant R$, and the equality holds when τ_R is constant. Here we develop a toy model in which the equality is valid for heterogeneous recovery time τ_R distribution but with constant transmissibility T_{τ_R}. This case is relevant in our study because we obtain that for a network with communities, there is not a strong dependence between the transmissibility T_{τ_R} and τ_R [see Fig. 4(c)].

To study the effect on the final state of a heterogeneous τ_R distribution with T_{τ_R} constant, we propose the following recovery time distribution

$$P(\tau_R) = 0.5\delta_{\tau_R,2} + 0.5\delta_{\tau_R,10}, \quad \text{(D17)}$$

where δ is the Kronecker delta, and the infection time distribution $P(\tau_I|\tau_R)$ is given by Table I, where $\sigma \in [0, 1]$.

For this case, $T = T_{\tau_R} = \sigma$. For the purpose of comparison, we also study a similar distribution $P(\tau_I|\tau_R)$ in which T_{τ_R} is not constant (see Table II).

Using the same recovery time distribution $P(\tau_R)$ as in the previous case, the transmissibilities are: $T_{\tau_R=2} = \sigma^{10}$, $T_{\tau_R=10} = \sigma$, and $T = 0.5\sigma + 0.5\sigma^{10}$.

In Figs. 13(a) and 13(b), we show R and Π obtained from the theory [Eqs. (D1)–(D16)] and simulations for the recovery and infection time distributions in Eqs. (D17) and Table II. Our results confirm that for a constant T_{τ_R}, the probability of an epidemic is equal to the fraction of recovered
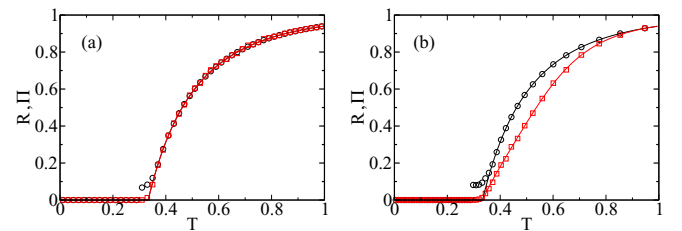

FIG. 13. Mapping between link percolation and the SIR model with heterogeneous recovery distribution for ER networks with $\langle k \rangle = 3$. The panels show R (black) and Π (red) as a function of the total transmissibility T for a heterogeneous recovery distribution given by Table I (a) and Table II (b). The lines correspond to the theoretical solutions of Eqs. (D2)–(D16), and the symbols to simulations. The simulations were performed over 10^4 network realizations with $N = 10^4$ and $s_c = 600$. The disagreement between the theoretical curves and the simulations around the critical point is due to finite size effects and the value of s_c which cannot distinguish an epidemic from an outbreak near $T = T_c$ (see Appendix A).

nodes [Fig. 13(a)] even if $P(\tau_R)$ is heterogeneous, while for nonconstant T_{τ_R}, $\Pi < R$ [Fig. 13(b)]. Thus, it is expected that

for a weak dependency between T_{τ_R} and τ_R, link percolation is a good approximation of the SIR model, as shown in Fig. 8.

[1] S. Fortunato, Phys. Rep. **486**, 75 (2010).

[2] A. Alexander-Bloch, R. Lambiotte, B. Roberts, J. Giedd, N. Gogtay, and E. Bullmore, Neuroimage **59**, 3889 (2012).

[3] M. Girvan and M. E. Newman, Proc. Natl. Acad. Sci. U.S.A. **99**, 7821 (2002).

[4] T. Zhou, M. Zhao, G. Chen, G. Yan, and B.-H. Wang, Phys. Lett. A **368**, 431 (2007).

[5] A. Arenas, A. Díaz-Guilera, J. Kurths, Y. Moreno, and C. Zhou, Phys. Rep. **469**, 93 (2008).

[6] W. Wang, Q.-H. Liu, J. Liang, Y. Hu, and T. Zhou, Phys. Rep. **820**, 1 (2019).

[7] A. Nematzadeh, E. Ferrara, A. Flammini, and Y.-Y. Ahn, Phys. Rev. Lett. **113**, 088701 (2014).

[8] F. Lazaridis, B. Gross, M. Maragakis, P. Argyrakis, I. Bonamassa, S. Havlin, and R. Cohen, Phys. Rev. E **97**, 040301(R) (2018).

[9] G. S. Fields, J. Dev. Econ. **2**, 165 (1975).

[10] K. H. Zhang and S. Shunfeng, Chin. Econ. Rev. **14**, 386 (2003).

[11] R. M. Anderson and R. M. May, *Infectious Diseases of Humans* (Oxford University Press, Oxford, 1992).

[12] L. D. Valdez, P. A. Macri, and L. A. Braunstein, PLoS ONE **7**, e44188 (2012).

[13] J. C. Miller, Infect. Dis. Model. **3**, 192 (2018).

[14] M. E. J. Newman, Phys. Rev. E **66**, 016128 (2002).

[15] L. J. Allen and A. M. Burgin, Math Biosci. **163**, 1 (2000).

[16] C. Lagorio, M. V. Migueles, L. A. Braunstein, E. López, and P. A. Macri, Physica A **388**, 755 (2009).

[17] D. Stauffer and A. Aharony, *Introduction to Percolation Theory*, revised 2nd ed. (CRC Press, Boca Raton, FL, 2014).

[18] A. Bunde and S. Havlin, *Fractals and Disordered Systems* (Springer, New York, 1991).

[19] R. Cohen, K. Erez, D. ben-Avraham, and S. Havlin, Phys. Rev. Lett. **85**, 4626 (2000).

[20] E. Kenah and J. M. Robins, Phys. Rev. E **76**, 036113 (2007).

[21] M. Salathé and J. H. Jones, PLOS Comput. Biol. **6**, e1000736 (2010).

[22] J. Hindes, S. Singh, C. R. Myers, and D. J. Schneider, Phys. Rev. E **88**, 012809 (2013).

[23] A. Vazquez, J. Theor. Biol. **245**, 125 (2007).

[24] V. Colizza and A. Vespignani, Phys. Rev. Lett. **99**, 148701 (2007).

[25] V. Colizza and A. Vespignani, J. Theor. Biol. **251**, 450 (2008).

[26] M. Barthelemy, C. Godreche, and J.-M. Luck, J. Theor. Biol. **267**, 554 (2010).

[27] P. Sah, S. T. Leu, P. C. Cross, P. J. Hudson, and S. Bansal, Proc. Natl. Acad. Sci. U.S.A. **114**, 4165 (2017).

[28] M. Nadini, K. Sun, E. Ubaldi, M. Starnini, A. Rizzo, and N. Perra, Sci. Rep. **8**, 2352 (2018).

[29] G. Dong, J. Fan, L. M. Shekhtman, S. Shai, R. Du, L. Tian, X. Chen, H. E. Stanley, and S. Havlin, Proc. Natl. Acad. Sci. U.S.A. **115**, 6911 (2018).

[30] L. D. Valdez, H. A. Rêgo, H. Stanley, and L. A. Braunstein, Sci. Rep. **5**, 12172 (2015).

[31] J. C. Miller, A. C. Slim, and E. M. Volz, J. R. Soc. Interface **9**, 890 (2011).

[32] M. E. J. Newman, S. H. Strogatz, and D. J. Watts, Phys. Rev. E **64**, 026118 (2001).

[33] L. A. Braunstein, Z. Wu, Y. Chen, S. V. Buldyrev, T. Kalisky, S. Sreenivasan, R. Cohen, E. Lopez, S. Havlin, and H. E. Stanley, Int. J. Bifurcat. Chaos **17**, 2215 (2007).

[34] This is since T is the parameter of our microscopic model, which controls the basic reproductive number [L. Meyers, Bull. Am. Math. Soc. **44**, 63 (2007)]. This magnitude, R_0, is a relevant measure in epidemiology to estimate the initial epidemic growth.

[35] R. Cohen, S. Havlin, and D. Ben-Avraham, in *Handbook of Graphs and Networks: From the Genome to the Internet*, edited by S. Bornholdt and H. G. Schuster (Wiley-VCH, Weinheim, 2003), Chap. 4, p. 85.

[36] E. Kenah and J. C. Miller, Interdiscip. Perspect. Infect. Dis. **2011**, 1 (2011).

[37] Setting that $\epsilon \neq 0$ means that the computation of R assumes that there is an epidemic.